LARGE EDDY SIMULATIONS AND PARTICLE IMAGE VELOCIMETRY EXPERIMENTS WITHIN A BIMHV FLOW NEAR PEAK SYSTOLE

Adam Blackmore

Department of Mechanical and Industrial Engineering
University of Toronto
5 Kings College Rd. Toronto, ON, M5S 3G8
ablackmore@hatch.ca

Pierre Sullivan

Department of Mechanical and Industrial Engineering
University of Toronto
5 Kings College Rd. Toronto, ON, M5S 3G8
sullivan@mie.utoronto.ca

ABSTRACT

Comparing previous experiments (Hutchison *et al.* (2011)), and high resolution Large Eddy Simulations on a BiMHV flow at peak systole show significant differences in the central jet of the BiMHV. The LES results show flow separation at the valve leaflets with regions of significant shear between the central and outer jets not seen in the measurements. This is primarily caused by measurement errors because of the difficulty of extracting data from regions of high shear and optical–matching issues using PIV. However, evidence of the four cell structure described by Hanle *et al.* (1988) for both continuous and pulsatile flow and Hutchison *et al.* (2011) for continuous flow was also found with the LES results, suggesting that more experiments are required at peak systole and there is a need for some cautions when moving forward with cyclic measurements. Specifically, more effort must be spent capturing the high shear region of the central jet, as well as measurement planes perpendicular to the longitudinal axis of the aortic chamber.

INTRODUCTION

The degeneration of mitral and aortic valves in the human heart results in thousands of heart valve replacement surgeries every year. This requires that an adequate replacement be available to physicians. The use of prosthetic mechanical heart valves is widespread, with the bi-leaflet mechanical design being the most popular. Unfortunately, these valves can create flow fields which produce damaging stress levels on the red blood cells (RBCs). This stress-induced damage can eventually result in serious medical complications such as thrombosis and RBC lysis. There clearly exists potential for an improved valve, which will require a thorough understanding of the fluid mechanics associated with a particular design.

With increased computing power, the use of computational fluid dynamics (CFD) to study complex flows has increased, and CFD will increasingly be an important tool for refining BiMHV designs. Many studies have shown that CFD can quantify major flow features associated with the flow downstream of a BiMHV (De Tullio *et al.* (2009); Ge *et al.* (2003, 2005)). Since CFD will become an important research tool in the development of new valve designs, it is necessary to validate computational results experimentally to ensure design calculations can be trusted. Due to the confined measurement region, the two most common measurement techniques used in the study of BiMHV flows are LDA and PIV. While LDA is a pointwise technique, PIV captures the whole flow field, and is ideally suited to provide benchmark experimental results for the validation of numerical methods. However, it requires substantial design preparations (fluid and optical access) in order to be able to perform measurements in this complex flow environment.

The primary physical feature that causes cell lysis and thrombosis of the RBCs is postulated to be the stress imposed on the RBC by the turbulent flow field. The threshold of stress which caused hemolysis was investigated by Lu *et al.* (2001) using two component Laser Doppler Anemometry (LDA) in a well-controlled steady jet flow. Jones (1995) studied the destruction of ethrocytes by turbulence and found that viscous dissipation could be more important in predicting cell damage than Reynolds stress. Ge *et al.* (2007) performed experiments and simulations of flow downstream of a BiMHV to compare viscous and Reynolds stress, and found that viscous stress was a better measure of the physical environment experienced by the RBC. This stress would act on the smallest scales of the flow due to the turbulent dissipation of the large scale coherent structures; thus, the correct determination of turbulent dissipation downstream of a BiMHV can lead to useful insights on valve performance.

However, turbulent dissipation is very difficult to measure. This is primarily due to the scales associated with the measurement, which are on the order of the Kolmogorov scale; complicating the determination of turbulent dissipation is the need to compute a number of derivatives from experimental data, which can lead to significant error. PIV with sub-grid scale models has been used in Large Eddy Simulation (LES) by Sheng *et al.* (2000) to obtain turbulent dissipation in a stirred reactor. The advantage of this ap-

proach was that it did not require the fine spatial resolution that would be needed to directly calculate the dissipation by differentiating velocity. Li *et al.* (2010) carried out a dissipation analysis using this method in a BiMHV flow, however the experiments were conducted in a pulsatile flow with relatively low sample sizes and no error analysis was presented to quantify the results. In BiMHV flows η has been estimated to be on the order of 10-100 μm (Jones (1995); Li *et al.* (2010); Lu *et al.* (2001)), which is far smaller than the spatial resolution of the current measurements. Sheng *et al.* (2000) presented dissipation rate calculations of PIV data from a stirred reactor using the Smagorinsky model from LES of turbulent flows. In a numerical simulation of turbulent flow using LES, the velocity field is low pass filtered, such that only the energy producing scales are resolved. The smaller scales are modeled, saving computational resources. All PIV methods are spatially averaged velocity estimates over a grid size determined by the experimental setup, therefore the measurements can be treated as a low pass filtered velocity field with a sharp cut–off below the grid resolution of the measurement. This method for predicting dissipation has the potential to be a valuable experimental tool, however there is a need for a formal evaluation of the error associated with the implementation as has been done by Ewing *et al.* (1995) for parallel hotwires. Since PIV does not generate enough of the velocity gradient terms for a full evaluation of the strain rate tensor it could be advantageous to couple the experiments with simulations to fill in the missing terms and compare estimates of dissipation and other higher–order terms.

The present paper compares flow downstream of a model BiMHV at peak systole using a well defined steady flow previously measured using stereoscopic PIV to a high–resolution data set obtained from fine–mesh Large Eddy Simulation. The present investigation will highlight potential regions of difficulty for PIV measurement, and present evidence of the need for further experimentation prior to applying the Large Eddy Simulation PIV technique to a BiMHV flow.

1 METHODOLOGY

Experiments were conducted within a recirculating test flow loop using Stereo Particle Image Velocimetry (SPIV), as described by Hutchison *et al.* (2011), which was constructed to investigate the flow characteristics of a BiMHV model operating in near peak systole conditions. Steady flow was provided by a centrifugal pump located upstream of the flow conditioning. The flow loop was operated in a steady flow mode to avoid cycle to cycle variations which would be present within a pulsatile flow investigation. In addition, the model BiMHV was set to a fixed opening angle of 87 degrees. This flow condition allows easier comparison with numerical models while minimizing errors with collecting sufficient data within pulsatile flows with valve leaflet movement. The flow conditioning upstream of the test section consisted of a honeycomb flow straightener, two turbulence screens and an axisymmetric contraction. This flow conditioning provided well defined inlet conditions, which can be used to evaluate numerical models. Before the test section there was 14.9d of inlet piping after the flow exited the contraction. The test section contained the model BiMHV, which was placed at the exit of the inlet piping. The aortic chamber was simulated by an axisymmetric model of size 1.19d which contracts to the aortic diameter
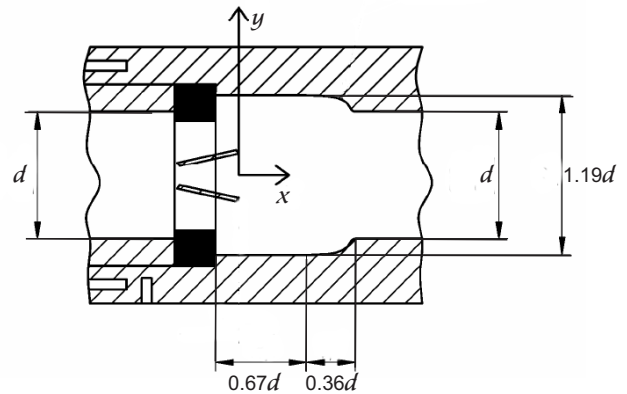
Figure 1. The test section

d. The test section was constructed of acrylic, and the exterior walls were flat in order to reduce the effect of optical distortions during experiments. As mentioned in Hutchison *et al.* (2011), the valve leaflet hinges were not part of the model, which consisted of polycarbonate leaflets encapsulated by an acrylic valve ring.

Stereo Particle Image Velocimetry Setup

Stereo Particle Image Velocimetry was used to calculate values of velocity for measurements downstream of the BiMHV. The system consisted of a New Wave SOLOPIV 120 mJ Nd:YAG laser, two(2) 1008×1018 pixel Pulnix TM1010 cameras, delay generator, function generator, personal computer with two(2) Bit-Flow Road Runner V12 frame grabbers and a logic box. The delay generator was used to control the Q-switching and delay pulse timing of the lasers during the measurements. A function generator was used to send a 3 Hz acquisition signal to the cameras, which acquired and stored images via Video Savant 3.0 software. The laser emitted light with a wavelength of 532 nm, and lenses were used to spread and focus the light sheet, which resulted in a light sheet thickness of approximately 1 mm during the measurements. The flow was seeded with silver coated hollow glass spheres, with a mean diameter of 15 μm. The SPIV described had resulted a resolution of approximately 0.59 mm in the x direction and 0.53 mm y direction. A diagram of the test section and location of the light sheet can be seen in Figure 2(a), and a diagram of the SPIV acquisition can be seen in Figure 2(b).

Computational Methodology

In the present investigation the results of the SPIV experiments are compared to high resolution LES. The filtered incompressible, isothermal conservation equations for mass, and momentum are:

$$\frac{\partial \rho}{\partial t} + \frac{\partial \rho \overline{U_i}}{\partial x_i} = 0 \qquad (1)$$

$$\frac{\partial \rho \overline{U_j}}{\partial t} + \frac{\partial \rho \overline{U_i U_j}}{\partial x_i} = \nu \frac{\partial^2 \overline{U_j}}{\partial x_i \partial x_i} - \frac{1}{\rho} \frac{\partial \overline{p}}{\partial x_j} \qquad (2)$$

SIDE VIEW   FRONT VIEW
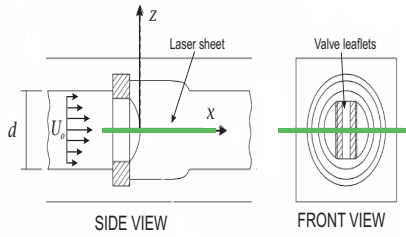
(a) Test section showing measurement plane
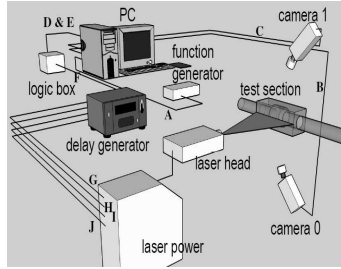
(b) SPIV set–up

Figure 2.   Experimental set–up and measurement plane of the SPIV

The conservation equations were discretized and solved using the finite volume method based commercial solver ANSYS FLUENT 14 (ANSYS, 2011). The filtered conservation equations were closed using the Smagorinsky-Lilly model Smagorinsky (1963); Lilly (1966) and modelled as:

$$\mu_t = \rho (L_s)^2 \|\overline{S}\| \qquad (3)$$

where L_s is determined based on

$$L_s = min(\kappa d*, C_s \triangle) \qquad (4)$$

where κ is the von Karman constant, d* is the distance to the nearest wall, C_s is the Smagorinsky-Lilly constant, which was set equal to 0.12 in the present investigation base on the analysis by Meneveau & Katz (2000); $\triangle$ is computed based on the cell volume, $V^{\frac{1}{3}}$. The conservation equations were solved using the segregated pressure based solver with an Algebraic Multigrid (AMG) method and Gauss-Seidel smoother for the linear system of equations. The Semi-Implicit Pressure Linked Equations (SIMPLE) algorithm of Patankar (1980) was used to iteratively solve the conservation equations. The momentum equation was discretized using a 2nd order bounded central differencing scheme, and the temporal terms were discretized using a 2nd order backwards implicit scheme. The time step was set to ensure that the Courant Number (Co) was below 0.3.
The simulations were matched to the experiment with a Re

based on the valve diameter of 7800. This resulted in a mean velocity, U_o of 0.32 m/s. The inlet condition was set as a mass flow inlet, and the outlet was set as a constant pressure outlet. The walls were considered no-slip, smooth
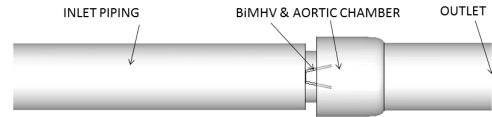
Figure 3.   The computational domain

wall boundaries, and the simulation was iso-thermal. Fully developed inlet conditions were created by first simulating the inlet section of the domain, and using periodic boundaries to build up turbulence and fully developed flow conditions. This was then used as a starting point for the simulations. The simulations were run for approximately 5 flow–through times, and statistics were then gathered for approximately 3.5 sec of flow time($\sim$ 42 integral time scales assuming $T_I = \frac{d}{U_o}$).

1.1   Computational Grid
The computational domain consisted of a straight section of inlet piping approximately 16.3 cm long, which was followed by the BiMHV and Aortic chamber, as described in Figure 1. The domain can be seen in Figure 3. The domain was discretized into purely hexahedral elements using a block based topology created in ANSYS ICEM version 14. The block based topology allowed the complex geometry of the valve to be meshed using purely hexahedral elements; o-grid type blocks were used to accurately control the distance from the cell to the wall. The maximum skewness of each mesh was 0.7 (orthogonal quality = 0.3). The first mesh consisted of approximately 0.6M cells, and the second mesh consisted of approximately 1.5M cells, and the third mesh contained approximately 3.7M cells. Table 1 provides details on each mesh. The computational mesh and blocking topology can be seen in 1.1 and 1.1.

Table 1.   Computational grid details.

Mesh	Number of Cells	Normalized Average Cell Size $L_{ave} = (V_{ave})^{\frac{1}{3}}$
Coarse	0.6×10^6	0.033d
Medium	1.5×10^6	0.015d
Fine	3.7×10^6	0.009d

1.2   Grid Independence
The ASME guidelines control of numerical accuracy (Celik *et al.*, 2008) were used to test the grid convergence. For this study the grid refinement factor , r, was 2.2 from the coarse to the medium grid and 1.7 from the medium to the fine grid exceeding the recommended value of 1.3. For the purposes of the study, the key variable, ϕ, was chosen as the average normalized peak velocity of the three jets in the mid–plane. The three jet structure is an important characteristic of the flow through a BiMHV at peak systole, and was chosen to demonstrate the numerical accuracy. The apparent order of the method, p, was 2.58 for both
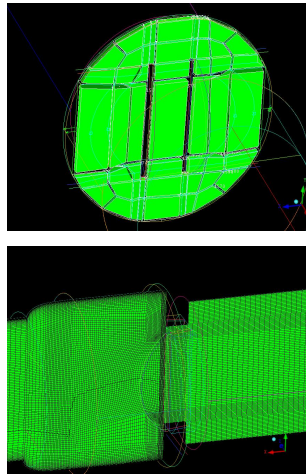
Figure 4.   Coarse grid slice and blocking structure

outer jets and 2.65 for the central jet. The results demonstrate that the numerical uncertainty based on the fine–grid convergence index, GCI_{Fine}, for the finest mesh of the left and right jet peaks is approximately 1.8%, and the center jet peak is approximately 2.6%. These results show the uncertainty associated with the grid resolution is well within acceptable range.

Table 2.   Grid convergence test results

Mesh	$\dfrac{U_{mean}}{U_o}$			L_{ave}	r
	Left Jet	Right Jet	Center Jet		
Coarse	2.15	2.15	1.9	0.033d	
Medium	2.6	2.6	2.6	0.0153d	2.2
Fine	2.5	2.5	2.45	0.009d	1.7
p	2.58	2.58	2.65		
GCI_{Fine}	0.018	0.018	0.026		

RESULTS

The time averaged results of velocity in the valve mid plane can be seen in Figure 5; the contours of mean axial velocity clearly show the characteristic three jet structure of the BiMHV flow. The left and right jets have a magnitude of approximately $2.6U_o$. The regions between the right and left jets, and the aortic wall show a region containing significant reversed flow; the maximum magnitude of this flow is approximately $0.8U_o$. This is significantly larger than the maximums detected in the experiment Hutchison *et al.* (2011), and is hypothesized to be due to the poor vector resolution near the wall; however, recirculation in the near wall region at the valve exit was measured in the experiments, and this compares well to the numerical results. The contours of W_{avg}/Uo show the flow expanding equally in each lateral direction, and compare well with the experimental results, which can be seen in Hutchison *et al.* (2011). The magnitudes and distribution of lateral velocity are similar, and reach maximums of $0.6U_o$.
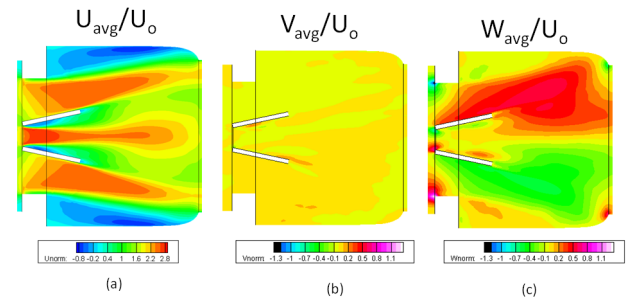
Figure 5.   Time–averaged velocity contours downstream of the valve chamber - Large Eddy Simulation

The central jet is influenced largely by the separation of the flow within the valve body. Two separation zones can be seen immediately downstream of the valve entrance; the velocity of the central jet reaches a maximum at this point. These results differ from the experimental results significantly. The velocity profiles of the numerical and experimental results 8 mm downstream of the valve tip are plotted in Figure 7. The experimental results show a more gradual change in velocity across the central jet region, which indicates the experiments did not detect any flow separation at the valve leaflets. From companion streak visualization performed by Hutchison (2009), the central jet had a paucity of seeding particles. With the adaptive windowing performed in the PIV measurements, it is likely that this biased the experiment in this region to the higher speed flow. It is likely that the numerical results presented here for this region are more reliable. The slight asymmetry in the experimental results are due to a slight variance in the inlet conditions of the experiment likely caused by the inlet conditions and settling of the aqueous sodium iodide solution used for refractive matching (discussed in Hutchison *et al.* (2011)); this asymmetry is not seen in the numerical results.

The experiments did not perform any measurements in the y–z plane, but the measurements of out–of–plane velocity captured in the SPIV data did contain evidence of a four cell flow structure downstream of the valve also seen by Hanle *et al.* (1988). The current simulations show evidence of the same four cell flow structure, Figure 6. The contour plots of $< R_{wv} >$ show eight flow structures immediately at the exit of the valve. The four central cells diminish rapidly, and are barely detectable at the midpoint of the aortic chamber. The four outer cells sustain over the entire aortic domain; this is postulated to be due to the large reversed flow areas at the right and left jets at the exit of the valve.

CONCLUSIONS

Experiments and numerical simulations were conducted on a BiMHV flow at peak systole. The experiments provided a well defined data set and were compared to numerical simulations. The key differences discovered in the experimental and numerical results is primarily related to the difference in mean axial velocity profiles where there is high shear. It is thought that this is the result of settling of the aqueous sodium iodide in the experiments as a number of checks had been performed on the mean pro-

4

$$WV_{avg}/U_o^2$$
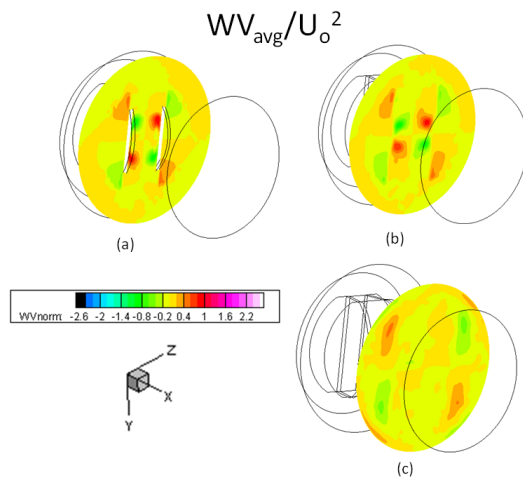
Figure 6. Time–averaged lateral Reynolds stresses R_{wv}, downstream of the valve chamber - Large Eddy Simulation
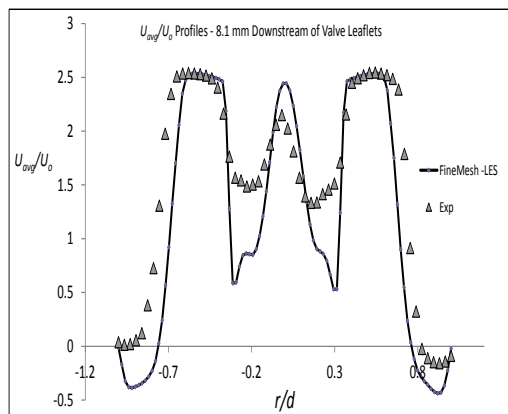
Figure 7. Experimental and LES time–averaged streamwise velocity profiles, U_{avg}/U_o, 8 mm downstream of the valve exit

file to ensure correct alignment. Contour plots of R_{wv} in the numerical investigation also presented evidence of the four cell structure detected by Hanle *et al.* (1988) and Hutchison *et al.* (2011). In addition, the simulations also demonstrated that four other cellular flow structures exist in the outer aortic chamber, which are primarily driven by the recirculation zones in that region. The present investigation demonstrates the complexity of the flow through a BiMHV, and highlights the need for further experimentation at peak systole. In particular, future experiments should focus on measurements in the y–z plane, and the central jet shear layer.

REFERENCES

ANSYS, Inc 2011 *ANSYS FLUENT 14 Guide*.

Celik, Ismail B, Ghia, Urmila, Roache, Patrick J, Freitas, Christopher J, Coleman, Hugh & Raad, Peter E 2008 Procedure for Estimation and Reporting of Uncertainty Due to Discretization in CFD Applications. *Journal of Fluids Engineering* **130** (7), 078001.

De Tullio, M. D., Cristallo, A., Balaras, E. & Verzicco, R. 2009 Direct numerical simulation of the pulsatile flow through an aortic bileaflet mechanical heart valve. *Journal of Fluid Mechanics* **622**, 259.

Ewing, D, Hussein, H J & George, W K 1995 Spatial resolution of parallel hot-wire probes for derivative measurements. *Experimental Thermal and Fluid Science* **11** (2), 155–173.

Ge, L., Dasi, L., Sotiropoulos, F. & Yoganathan, A. 2007 Characterization of hemodynamic forces induced by mechanical heart valves: Reynolds vs. Viscous stress. *Annals of Biomedical Engineering* **36**.

Ge, L., Jones, S., Sotiropoulos, F., Healy, T. & Yoganathan, A. 2003 Numerical Simulation of Flow in Mechanical Heart Valves: Grid Resolution and the Assumption of Flow Symmetry. *Journal of Biomechanical Engineering* **125** (5), 709.

Ge, L., Leo, H.L., Sotiropoulos, F. & Yoganathan, A. 2005 Flow in a Mechanical Bileaflet Heart Valve at Laminar and Near-Peak Systole Flow Rates: CFD Simulations and Experiments. *Journal of Biomechanical Engineering* **127** (5), 782.

Hanle, D. D., Harrison, E.C., Yoganathan, A.P. & Corcoran, W.H. 1988 In Vitro Fluid Dynamics of the St. Jude Valve Prosthesis in Steady and Pulsatile Flow. *Engineering in Medicine* **17(4)**, 181–187.

Hutchison, Christopher 2009 Stereoscopic PIV In Steady Flow Through a Bileaflet Mechanical Heart Valve.

Hutchison, Chris, Sullivan, Pierre & Ethier, C Ross 2011 Measurements of steady flow through a bileaflet mechanical heart valve using stereoscopic PIV. *Medical & biological engineering & computing* **49** (3), 325–35.

Jones, S. 1995 A relationship between Reynolds stresses and viscous dissipation: implications to red cell damage. *Annals of Biomedical Engineering* **23** (1), 21–8.

Li, C.P., Lo, C.W. & Lu, P.C. 2010 Estimation of viscous dissipative stresses induced by a mechanical heart valve using PIV data. *Annals of Biomedical Engineering* **38** (3), 903–16.

Lilly, D K 1966 On the application of the eddy viscosity concept in the inertial sub–range of turbulence. *Tech. Rep.* NCAR Manuscript 123. Boulder, CO.

Lu, P.C., Lai, H.C. & Liu, J.S. 2001 A reevaluation and discussion on the threshold limit for hemolysis in a turbulent shear flow. *Journal of Biomechanics* **34** (10), 1361–4.

Meneveau, Charles & Katz, Joseph 2000 Scale-Invariance and Turbulence Models for Large-Eddy Simulation. *Annual Review of Fluid Mechanics* **32** (1), 1–32.

Patankar, Suhas V 1980 *Numerical Heat Transfer and Fluid Flow*, 1st edn. Washington, DC: Hemisphere Publishing Corp.

Sheng, J., Meng, H. & Fox, R.O. 2000 A large eddy PIV method for turbulence dissipation rate estimation. *Chemical Engineering Science* **55**, 4423–4434.

Smagorinsky, J 1963 General Circulation Experiments with the Primitive Equations: 1. The Basic Experiment. *Monthly Weather Review* **91** (3), 99–164.